Softening of a reststrahlen band in CuO near the Néel transition

C.C. Homes, M. Ziaei,* B.P. Clayman, and J.C. Irwin
Department of Physics, Simon Fraser University, Burnaby, British Columbia, Canada V5A 1S6

J.P. Franck
Department of Physics, University of Alberta, Edmonton, Alberta, Canada T6G 2J1
(Received 20 June 1994; revised manuscript received 12 September 1994)

The reflectance of sintered powders and single crystals of cupric oxide (CuO) has been measured from $\approx$ 50 to 3000 cm^{-1} as a function of temperature, above and below the magnetic-ordering transitions. For the sintered materials, the effect of ^{65}Cu and ^{18}O isotope substitutions on the phonon frequencies was studied. For single crystals, radiation was polarized both parallel ($E \parallel c$) and perpendicular ($E \perp c$) to the c axis in the [1$\bar{1}$0] growth plane. The single-crystal reflectance results have been reproduced extremely well using a modified dispersion-analysis model. In the sintered powders, and for $E \perp c$ in the single crystals, a strong reststrahlen band is observed to soften dramatically at $T_{N1} \approx 230$ K, while below the commensurate antiferromagnetic-ordering transition at $T_{N2} \approx 213$ K the band hardens monotonically. However, no new phonon structure is observed in the antiferromagnetically ordered ground state, indicating that there is no superlattice in the direct lattice below T_{N2}. There is also a large transfer of oscillator strength below T_{N2} among the three high-frequency copper-oxygen vibrations; similar behavior is observed in the c-axis phonons of the oxygen-reduced high-T_c cuprate $YBa_2Cu_3O_{6+x}$ ($x \approx 0.6$); it is argued that the underlying mechanisms for the phonon anomalies in these two systems may be related.

I. INTRODUCTION

Since the discovery of high-temperature superconductivity in cuprate-based materials, there has been a considerable effort to study the lattice vibrations in these materials to gain an understanding of the nature of the electron-phonon coupling.[1] While it is generally accepted that the interactions between the Cu and O atoms in the square (or almost square) configuration found in the CuO_2 planes plays a decisive role in high-temperature superconductivity, there is still no common understanding of the pairing mechanism. In cupric oxide (CuO), where the atoms are planar coordinated in slightly distorted squares, the copper-oxygen coordination and separation are similar to that of many cuprate-based superconductors, suggesting that CuO may comprise a simple system in which to study the copper-oxygen interactions that may be important in high-temperature superconductivity. This suggestion has resulted in a number of recent investigations of the thermal,[2] electronic,[3] magnetic,[4–6] and optical[7–15] properties of CuO. Neutron-scattering experiments have found that the Cu^{2+} spins order incommensurately below $T_{N1} = 230$ K, and then order commensurately into an antiferromagnetic (AF) ground state along the [10$\bar{1}$] directions of the crystal below $T_{N2} = 213$ K, leading to a doubling of the magnetic unit cell along the a and c directions; the magnetization is in the [010] direction.[4]

Although the magnetic and transport properties of CuO powders and single crystals are well known, the optical properties have only been studied recently. Raman-scattering experiments[7–11] have been performed on sintered powders and single crystals. Infrared studies on sintered powders have examined the reflectance at room temperature,[12] as well as the temperature dependence of the reflectance[13] and transmission.[14] The polarized reflectance of a single crystal has been performed only at room temperature.[15] Kliche and Popovic[13] have observed a broad mode at $\approx$ 410 cm^{-1} in the reflectance of sintered powders, whose intensity was observed to change dramatically below T_{N2}. Raman studies on sintered powders as well as single crystals have also revealed the presence of a new feature at $\approx$ 240 cm^{-1} in the AF-ordered ground state; both the infrared and Raman results have been discussed in terms of having magnetic origins. However, transmission studies and the polarized reflectance of single crystals show no sign of a band in the $\approx$ 410 cm^{-1} region at room temperature. Furthermore, a direct comparison of two room-temperature studies of the reflectance of cupric oxide[12,13] indicates that there is some disagreement over the structure associated with the high-frequency phonons.

We have measured the polarized reflectance of a single crystal of CuO with the electric field polarized parallel and perpendicular to the crystallographic c axis in the [1$\bar{1}$0] growth plane, from $\approx$ 50 cm^{-1} to 3000 cm^{-1} as a function of temperature above and below the magnetic-ordering transition(s); we have also performed similar (unpolarized) measurements on sintered powders. The polarized reflectance of the monoclinic single crystal has been interpreted using a modified dispersion-analysis model for the dielectric function[15] and the agreement with the experimental data is excellent. A broad reststrahlen band centered at $\approx$ 450 cm^{-1} is found to be

strongly temperature dependent near T_{N1} and T_{N2}. Furthermore, below the Néel transitions there is a transfer of oscillator strength away from the transverse optic mode associated with the strong reststrahlen band to the other high-frequency copper-oxygen vibrations. In this work, the results from the sintered powders and the single crystals are consistent, and show no evidence of any new structures in the AF-ordered ground state — a result which differs from the work of Kliche and Popovic. The reststrahlen (residual ray) band usually refers to a single prominent feature in the reflectance due to the strong splitting in ionic crystals of the transverse optic (TO) and longitudinal optic (LO) modes, as is seen in simple alkali-halide crystals.[16] However, in a more complex system such as CuO, there are several optically active vibrations; we will refer only to the strongest feature near 450 cm^{-1} as the reststrahlen band.

II. EXPERIMENTAL DETAILS

A. Crystal structure

The crystal structure of cupric oxide is monoclinic, with four CuO units in the unit cell, as shown in Fig. 1. The monoclinic unit cell belongs to the space group $C_{2h}^6(C2/c)$, with the room-temperature unit cell dimensions[18] $a = 4.6837$ Å, $b = 3.4226$ Å, $c = 5.1288$ Å, $\alpha = \gamma = 90°$, and $\beta = 99.54°$. The structure can be viewed as consisting of chains along the $[10\bar{1}]$ and [101] directions.

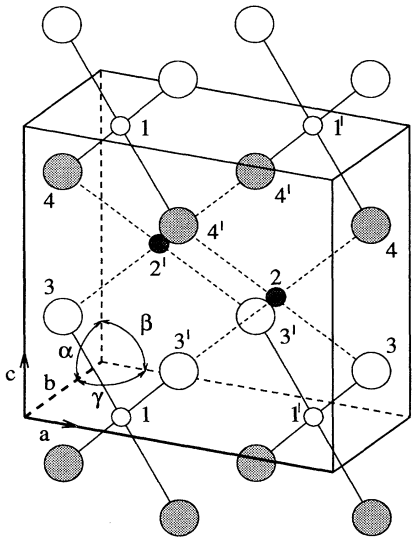

FIG. 1. The monoclinic unit cell of CuO. There are four formula units in the crystallographic unit cell, but only two in the primitive cell. The copper atoms are denoted by the small circles (1,2), while the oxygen atoms are the large circles (3,4); symmetrically equivalent positions are indicated by a prime. The different shades given to the copper and oxygen atoms, as well as the solid and dotted lines, illustrate the planar coordination of the oxygen atoms around the copper atom. The structure can be viewed as consisting of chains along the $[10\bar{1}]$ direction in which the Cu-O-Cu angle is 146°; Cu-O-Cu bond angles in the [101] direction are all less than 109°.

The primitive cell contains two molecular units and thus there are 12 vibrational modes. The Cu atoms are located on sites with C_i symmetry and the O atoms on sites with C_2 symmetry. A factor group analysis of the unit cell[9] yields the irreducible representations for the ($\mathbf{q} = 0$) vibrational modes:

$$\Gamma = 4A_u + 5B_u + A_g + 2B_g.$$

The three acoustic modes are represented by $A_u + 2B_u$, the six $3A_u + 3B_u$ modes are infrared active, and the three $A_g + 2B_g$ modes are Raman active. The Raman-active modes have been observed at 303 cm^{-1} (A_g), 350 cm^{-1} (B_g^1), and 636 cm^{-1} (B_g^2).[9] The A_u modes are oriented along the b-axis direction, while the B_u modes have different orientations in the ac plane. The $^{63}Cu^{16}O$, $^{63}Cu^{18}O$, and $^{65}Cu^{16}O$ powders used in this work were obtained from MSD Isotopes, a division of Merck Frosst Canada Inc. The specified isotopic purity of the ^{65}Cu and ^{18}O samples is > 99 at. %. The powders were pressed into pellets about 5 mm in diameter using a pressure of about 14 kbar. The $^{63}Cu^{16}O$ and $^{65}Cu^{16}O$ pellets were then sintered in air at 950 °C for about 18 h, while the $^{63}Cu^{18}O$ sample was sintered in an $^{18}O_2$ atmosphere. Single crystals of cupric oxide were prepared by flux growth with CuO, V_2O_5, MoO_3, and K_2CO_3 as the starting materials. The flux composition and growth temperatures were identical to those used by Wanklyn and Garrard,[17] with a cooling rate of 6 K per hour. The crystals obtained were irregularly shaped, and varied in size with the largest being approximately $3 \times 5 \times 10$ mm^3.

B. Reflectance

The reflectance was measured at a near-normal angle of incidence for sintered powders and single-crystal samples of CuO on a Bruker IFS 113V Fourier-transform interferometer from ≈ 50 to 3000 cm^{-1}. In the far infrared, a pyroelectric DTGS detector was used, while in the midinfrared, an MCT detector was used. The single crystal of CuO was glued to the apex of a pyramidal cone so that light is incident on the $[1\bar{1}0]$ growth face; the sintered powders were similarly mounted. To ensure good thermal contact, the brass cone holding the sample was anchored with copper braid to the cold finger of the flow dewar. An overfilling technique[19] was used so that light that missed the sample was scattered out of the optical path. For the sintered powders, the light was unpolarized. For the single-crystal samples, a Cambridge Physical Sciences IGP 223 polarizer was used in the region below 500 cm^{-1}; above this region an IGP 225 polarizer was used. The radiation is polarized both parallel and perpendicular to the c axis. However, because the polarizer is aligned by eye along the crystal-growth direction, there is a small (±5%) error associated with the accuracy of the polarization.

The reflectance of the sample (R_s) was compared to the reflectance of a stainless-steel reference mirror (R_m).

To correct for the sample size and any irregularities in the surface, and to eliminate the effects of the reference mirror, the sample was overcoated with gold *in situ*, and the measurements were repeated on the gold-coated sample (R_{gs}). The effects of the reference mirror may be removed by dividing these two ratios,

$$\left(\frac{R_s}{R_m}\right)\left(\frac{R_{gs}}{R_m}\right)^{-1} = \frac{R_s}{R_{gs}},$$

which yields the reflectance of the sample with respect to gold. The reflectance for gold is well known,[20] and the reflectance may subsequently be corrected by multiplying the ratio by the reflectance of gold to yield the absolute reflectance of the sample. The accuracy of the absolute reflectance is estimated to be ±1%.

III. DISPERSION ANALYSIS

For crystals with orthorhombic or higher symmetry, the dielectric tensor can be reduced to a diagonal form, and its principal axes coincide with the crystal axes. In the case of a monoclinic crystal, only one principal axis of the dielectric tensor coincides with a crystal axis (b axis). The other two principal axes lie in the ac plane, and their directions can change with frequency.[21] As a result, the dielectric tensor cannot be diagonalized simultaneously for all frequencies. This precludes a complete analysis of the reflectance using the Kramers-Kronig method. Similarly, simple models based on Lorentzian or factorized forms of the dielectric function fail to consider the nondiagonal form of the dielectric tensor.

A dispersion-analysis model for the light reflected from the ac plane of a monoclinic crystal has been reported by Belousov and Pavinich,[22,23] and extended to other crystals.[24] Using the dispersion-analysis model, the dielectric tensor in the ac plane can be written as

$$\epsilon_{xx}(\omega) = \epsilon_{xx}(\infty) + \sum_{i=1}^{3} \frac{\omega_{pi}^2 \cos^2\phi_i}{\omega_i^2 - \omega^2 - i\omega\gamma_i}, \tag{1}$$

$$\epsilon_{zz}(\omega) = \epsilon_{zz}(\infty) + \sum_{i=1}^{3} \frac{\omega_{pi}^2 \sin^2\phi_i}{\omega_i^2 - \omega^2 - i\omega\gamma_i}, \tag{2}$$

$$\epsilon_{xz}(\omega) = \epsilon_{xz}(\infty) + \sum_{i=1}^{3} \frac{\omega_{pi}^2 \cos\phi_i \sin\phi_i}{\omega_i^2 - \omega^2 - i\omega\gamma_i}, \tag{3}$$

and

$$\epsilon_{yy}(\omega) = \epsilon_{yy}(\infty) + \sum_{j=1}^{3} \frac{\omega_{pj}^2}{\omega_j^2 - \omega^2 - i\omega\gamma_j}, \tag{4}$$

where the $\omega_{i(j)}$, $\gamma_{i(j)}$, and $\omega_{pi(j)}$ are the TO frequencies, widths, and effective plasma frequencies of the B_u (A_u) modes, and $\epsilon_{xx}(\infty)$, etc., are the high-frequency dielectric constants for the various tensor components. The A_u vibrations are active only for polarizations along the b axis, and thus only contribute to ϵ_{yy}. The B_u oscillations are active in the ac plane, but the eigenvectors of these modes do not point along a principal crystalline axis. Consequently, the B_u vibrations are characterized by an additional parameter ϕ_i, which is the angle between the atomic displacement vectors and the x axis (see Fig. 2).

The reflectance at normal incidence from the ac plane is expressed as

$$R(\omega) = |r_{xx}|^2 + |r_{xz}|^2, \tag{5}$$

where

$$r_{xx} = \frac{(\tilde{n}_2^2 - \epsilon_{xx})r_1 - (\tilde{n}_1^2 - \epsilon_{xx})r_2}{\tilde{n}_2^2 - \tilde{n}_1^2}, \tag{6}$$

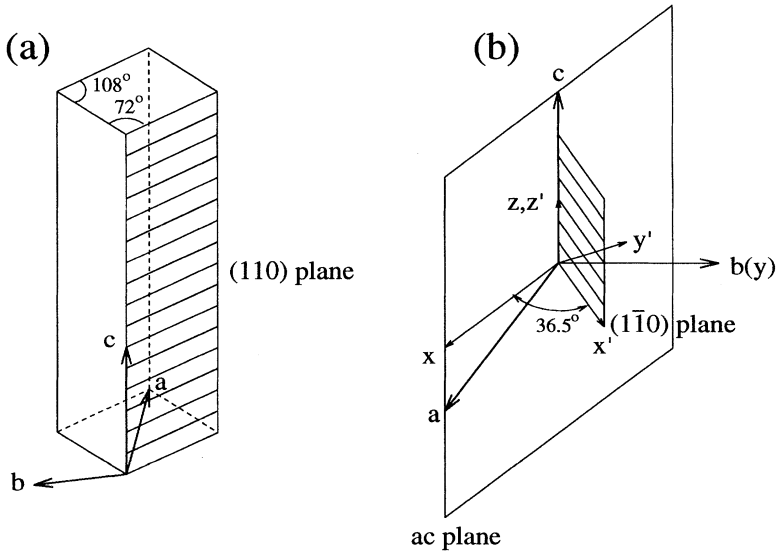

FIG. 2. (a) The as-grown single-crystal geometry. The crystallographic a, b, and c axes are shown. The b and c axes lie in the plane of the paper, while a points into the paper. (b) The geometry used for the infrared experiments. The a, b, and c axes are as shown in (a), while the x, y, and z axes form an orthogonal system, where y and z lie along the b and c directions, while x lies in the ac plane. The ac plane is rotated by 36.5° about the c axis into the [1$\bar{1}$0] plane; the resulting x', y', and z' refer to an orthogonal system in the [1$\bar{1}$0] plane. For the polarized reflectance experiments, the radiation was polarized both parallel and perpendicular to the c axis in the [1$\bar{1}$0] plane.

$$r_{xz} = \frac{-2\epsilon_{xz}}{(\tilde{n}_2 + \tilde{n}_1)(1 + \tilde{n}_1)(1 + \tilde{n}_2)}, \quad (7)$$

$$r_i = \frac{(1 - \tilde{n}_i)}{(1 + \tilde{n}_i)} \qquad (i = 1, 2), \quad (8)$$

and

$$(\tilde{n}_{1,2})^2 = (\epsilon_{xx} + \epsilon_{zz})/2 \pm \sqrt{(\epsilon_{xx} - \epsilon_{zz})^2/4 + \epsilon_{xz}^2}. \quad (9)$$

This model has been extended for the reflectance of the $[1\bar{1}0]$-type plane of a monoclinic crystal by Guha *et al.*,[15] by transforming the dielectric tensor from the xyz coordinate system into the $x'y'z$ coordinate system (as shown in Fig. 2), using a rotation angle of $\theta = 36.54°$ about the z axis; the new tensor components are

$$\epsilon'_{x'x'} = \cos^2\theta\epsilon_{xx} + \sin^2\theta\epsilon_{yy},$$

$$\epsilon'_{x'z'} = \cos\theta\epsilon_{xz},$$

and

$$\epsilon'_{z'z'} = \epsilon_{zz},$$

so that the reflectance in the $[1\bar{1}0]$ plane for $E \perp c$ is

$$R'(\omega) = |r_{x'x'}|^2 + |r_{x'z'}|^2. \quad (10)$$

Because of the presence of the ϵ_{yy} term in $\epsilon'_{x'x'}$, both the A_u and B_u modes will be observed for $E \perp c$. The frequencies described in Eqs. (1)–(4) are no longer pure TO modes as in the ac plane; instead they now describe modes with a mixed transverse optic-longitudinal optic (TO-LO) character. The reflectance for $E \parallel c$ is obtained by rotating the new dielectric tensor components about the y' axis by 90°.

IV. RESULTS

A. Sintered powders

The reflectance of sintered powders of CuO is shown in Fig. 3 for four temperatures, (a) above T_{N1} (295 K), (b) at $\approx T_{N2}$ (210 K); the remaining two temperatures (c) 170 K, and (d) 80 K are well below T_{N2}; other measurements were made at 250, 225, 200, 140, and 110 K. The room-temperature reflectance of sintered samples with ^{65}Cu and ^{18}O isotopes is shown in Figs. 4(a) and 4(b), respectively. The room-temperature reflectance data for the sintered powders in Figs. 3 and 4 are very similar. A strong reststrahlen band is seen clearly at ≈ 450 cm^{-1} at room temperature, where the reflectance reaches a maximum of nearly 60%. This measurement is consistent with the result of Degiorgi *et al.*[12] As the temperature is lowered to $\approx T_{N1}$, this feature appears to soften and broaden somewhat; finally, below T_{N2} the reststrahlen band appears to narrow, as do a number of other features.

The introduction of the dispersion-analysis model points out that because the dielectric tensor cannot

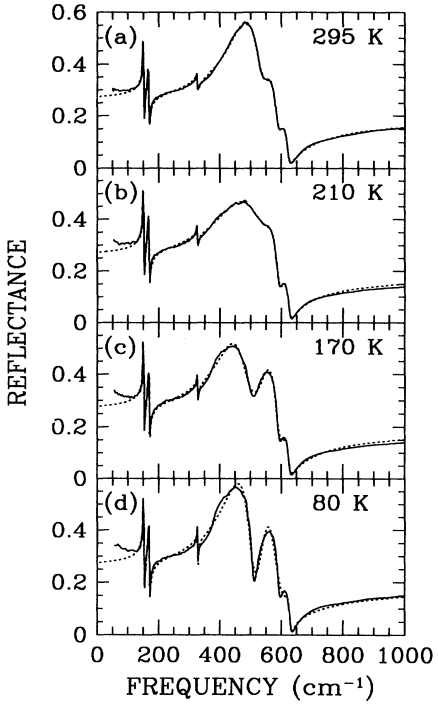

FIG. 3. The reflectance of the sintered sample of CuO from ≈ 50 to 1000 cm^{-1}, at (a) 295, (b) 210, (c) 170, and (d) 80 K. Due to the randomly oriented polycrystalline nature of the sample, all six infrared-active vibrations are seen. The dotted line is the fit to the factorized form of the dielectric function (see Table I).

be diagonalized simultaneously for all frequencies, the Kramers-Kronig analysis will not be complete. Nonetheless, the Kramers-Kronig analysis still provides valuable information; the only caution to interpreting the results is that the vibrations are not pure TO modes, but have a mixed TO-LO character, and thus the vibrational parameters of these features should not be confused with those of the pure TO modes. Bearing this in mind, the optical properties have been calculated by a Kramers-Kronig transformation of the reflectance, which yields the real and imaginary parts of the dielectric function

$$\tilde{\epsilon}(\omega) = \epsilon_1(\omega) + \epsilon_2(\omega) = \epsilon_1(\omega) + \frac{4\pi i}{\omega}\sigma_1(\omega), \quad (11)$$

where $\epsilon_1(\omega)$ and $\sigma_1(\omega)$ are the real parts of the dielectric function and optical conductivity, respectively. The extrapolations to high and low frequency were performed as follows: At low frequency the reflectance was assumed to be constant below the lowest measured frequency; at high frequency the data have been extended to $\approx 3\times10^4$ cm^{-1} using the data of Karlsson *et al.*[25] on sintered powders of cupric oxide, while above this frequency a free-electron behavior was assumed: $R \propto \omega^{-4}$.

The optical conductivity and the loss function (calculated from a Kramers-Kronig analysis of the reflectance curves in Fig. 3) are shown in Figs. 5(a) and 5(b), respectively. Usually, the peaks in the optical conductivity

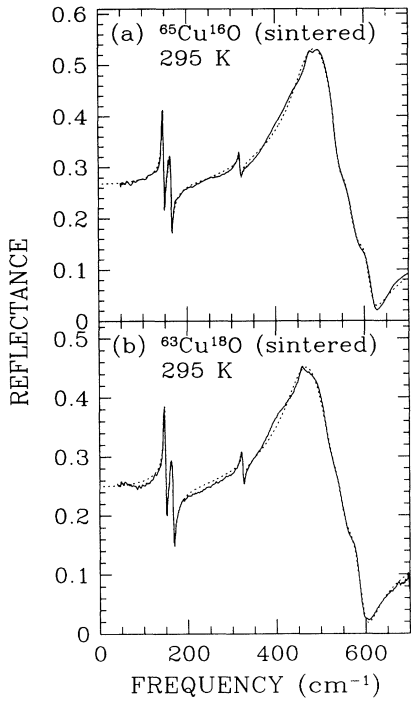

FIG. 4. The reflectance at room temperature of (a) the sintered powder of $^{65}Cu^{16}O$ and (b) the pressed powder of $^{63}Cu^{18}O$ (solid lines). The dotted lines in each of the panels represents the fit to the factorized form of the dielectric function (see Table I).

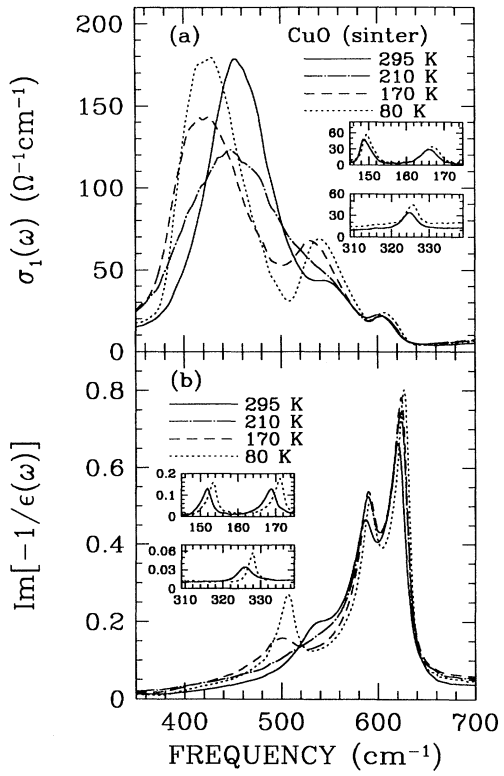

FIG. 5. The (a) optical conductivity and (b) loss function for the sintered sample of CuO at 295, 210, 170, and 80 K. The optical properties were obtained from a Kramers-Kronig analysis of the reflectance curves in Fig. 3. The peaks in $\sigma_1(\omega)$ and in the loss function indicate the positions of the TO and LO modes, respectively. Note that the TO and LO modes associated with the strong reststrahlen band in $\sigma_1(\omega)$ at ≈ 450 cm^{-1}, and in the loss function at ≈ 540 cm^{-1}, soften considerably below T_{N1}. Insets: the three low-frequency phonons, shown at 295 (solid line) and 80 K (dotted line).

identify the TO modes and the peaks in the loss function the LO modes, but in this case they refer to vibrations with a mixed TO-LO character. From group theory, there are a total of six allowed infrared-active modes, and six modes are indeed observed in the optical conductivity. The lower three phonons are quite sharp [as shown in the insets in Figs. 5(a) and 5(b)], and harden with decreasing temperature, displaying no unusual behavior near either T_{N1} or T_{N2}. As is evident in the reflectance, the conductivity is dominated by a feature associated with a strong reststrahlen band at ≈ 450 cm^{-1} at 295 K; this mode softens near T_{N1}, and appears to become broader, while below T_{N2} the mode narrows. The other two modes at high frequency both appear to soften somewhat. However, the large oscillator strength and width of the TO mode associated with the reststrahlen band make an absolute determination of the frequencies difficult. The loss function also shows three phonons in the same frequency region; in particular the mode at ≈ 540 cm^{-1} softens dramatically below T_{N1}, and it is clear that this feature is associated with the TO mode at ≈ 450 cm^{-1} in σ_1; the other two modes appear to harden slightly, but otherwise change very little.

B. Single crystal

The reflectance of a single crystal of CuO has been measured from the as-grown [1$\bar{1}$0] plane as a function of temperature, for radiation polarized parallel and perpendicular to the c axis.

1. $E \parallel c$

The reflectance of a single crystal of CuO for $E \parallel c$ (see Fig. 2) at 295, 210, 170, and 80 K is shown in Fig. 6; other measurements were made at 250, 225, 200, 140, and 110 K. An indication that the c axis is perpendicular to a principal optical axis is the fact that, unlike the sintered powders, where both the A_u and B_u modes are observed, only the three B_u modes are seen to be strongly active for $E \parallel c$. However, as noted above, because of the low symmetry of the system, these modes are no longer pure TO modes. The optical conductivity and loss function (calculated from the reflectance curves in Fig. 6) are shown in Figs. 7(a) and 7(b), respectively. The strong features at ≈ 520 cm^{-1} in $\sigma_1(\omega)$ and ≈ 620 cm^{-1} in the loss function harden slightly with decreasing temperature, and show no anomalous behavior at T_{N1} or T_{N2}.

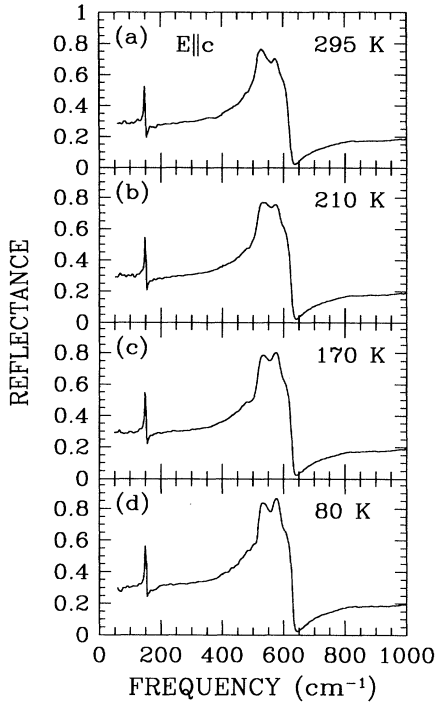

FIG. 6. The reflectance of single-crystal CuO for $E \parallel c$, from $\approx$ 50 to 1000 cm^{-1} at 295, 210, 170, and 80 K. Note that only the three B_u modes are expected to be active for this polarization.

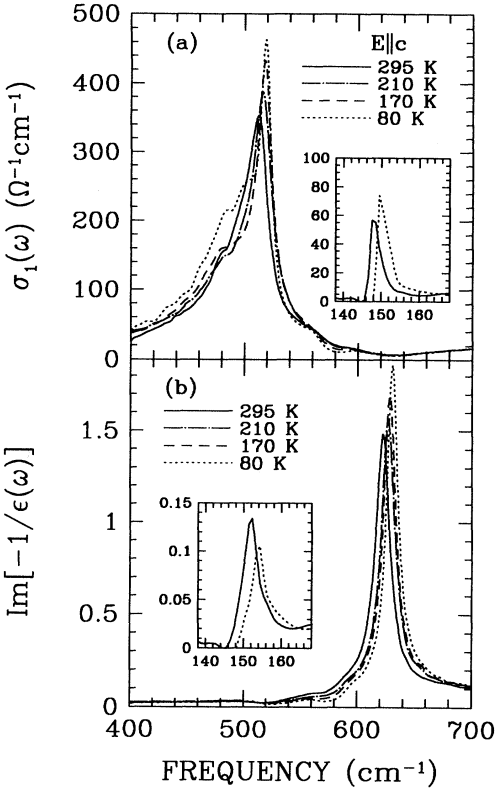

FIG. 7. The (a) optical conductivity and (b) loss function for a single crystal of CuO for $E \parallel c$, from 400 to 700 cm^{-1}, at 295, 210, 170, and 80 K, calculated from a Kramers-Kronig analysis of the reflectance curves in Fig. 5. Inset: the structure in the low-frequency region at 295 (solid line) and 80 K (dotted line).

The sharp low-frequency mode also fails to display any anomalous behavior at low temperature. The remaining feature, which was so prominent in the reflectance, is seen only as a weak shoulder in $\sigma_1(\omega)$ at $\approx$ 560 cm^{-1} and at $\approx$ 600 cm^{-1} in the loss function.

2. $E \perp c$

The reflectance of a single crystal of CuO for $E \perp c$ (see Fig. 2), at 295, 210, 170, and 80 K is shown in Fig. 8; other measurements were made at at 250, 225, 200, 140, and 110 K. Both the A_u and B_u modes are expected to be active for this polarization, and at least five are clearly visible in the reflectance. Unlike the $E \parallel c$ reflectance, there is a strong temperature dependence in the feature at $\approx$ 450 cm^{-1}. The optical conductivity and loss function (calculated from the reflectance curves in Fig. 8) are shown in Figs. 9(a) and 9(b), respectively. The strong, sharp feature seen in $\sigma_1(\omega)$ at $\approx$ 450 cm^{-1} is strongly temperature dependent, and softens considerably below T_{N1}; below T_{N2} it is observed to harden monotonically with decreasing temperature. Similar behavior is seen for the feature at $\approx$ 540 cm^{-1} in the loss function; these features are associated with a reststrahlen band in CuO, and its behavior in the single crystal is consistent with that seen in the sintered powder. The three low-frequency phonons [shown in the insets in Figs. 9(a) and 9(b)] harden slightly at low temperature, but display no anomalous temperature dependence at either T_{N1} or T_{N2}.

V. DISCUSSION

The polarized reflectance measurements of a single crystal of cupric oxide clearly show that the optical properties of this material are anisotropic. Because the sintered powder contains randomly oriented crystallites, they display a complicated reflectance spectra; this does not allow the application of the dispersion-analysis model. While the Lorentzian form of the dielectric function fails to describe the reflectance of the sintered powders, the factorized form describes the bulk features of the room-temperature reflectance quite well (as shown in the panels in Figs. 3 and 4), and has been successfully applied to other oxide systems.[26] However, because the factorized form of the dielectric function does not take into consideration the nondiagonal form of the dielectric tensor, this analysis is not definitive (as the failure to reproduce the fine structure at low temperature shows).

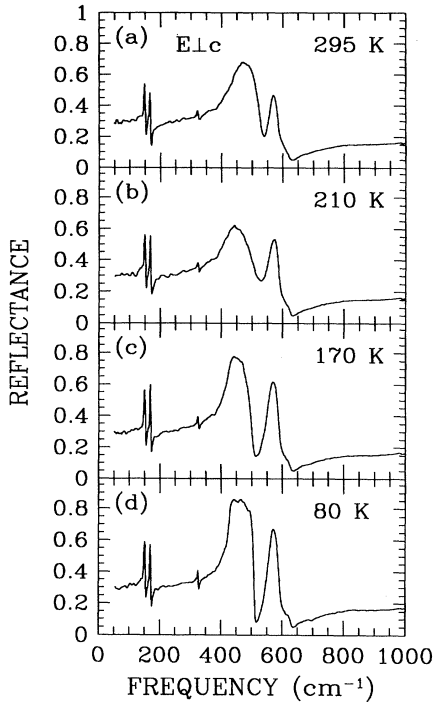

FIG. 8. The reflectance of single crystal CuO for $E \perp c$ on the $[1\bar{1}0]$ growth face, from $\approx$ 50 to 1000 cm^{-1} at 295, 210, 170, and 80 K. In this polarization, both the A_u and the B_u modes are expected to be infrared active.

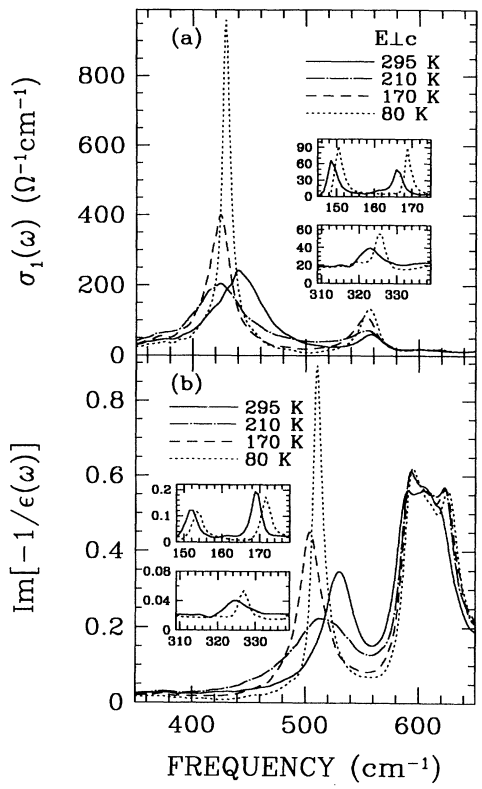

FIG. 9. The (a) optical conductivity and (b) loss function for a single crystal of CuO for $E \perp c$ on the $[1\bar{1}0]$ growth face, from 350 to 650 cm^{-1} at 295, 210, 170, and 80 K, calculated from a Kramers-Kronig analysis of the reflectance curves in Fig. 7. The strong, sharp features in $\sigma_1(\omega)$ and in the loss function are observed to soften at T_{N1}. Inset: the three low-frequency phonons at 295 (solid line) and 80 K (dotted line).

The factorized form of the dielectric function written as[27]

$$\tilde{\epsilon}(\omega) = \epsilon_\infty \prod_j \frac{\omega_{\mathrm{LO},j}^2 - \omega^2 - i\omega\gamma_{\mathrm{LO},j}}{\omega_{\mathrm{TO},j}^2 - \omega^2 - i\omega\gamma_{\mathrm{TO},j}}, \qquad (12)$$

where $\omega_{\mathrm{LO},j}$, $\omega_{\mathrm{TO},j}$, $\gamma_{\mathrm{LO},j}$, and $\gamma_{\mathrm{TO},j}$ are the frequencies and widths of the jth LO and TO modes, respectively. The factorized form has been fitted to the reflectance using a least-squares technique; the results of the fits to the room-temperature reflectance of cupric oxide, as well as for the ^{65}Cu and ^{18}O isotopic substitutions, are summarized in Table I. The fits quantify what was apparent in Figs. 5(a) and 5(b), namely, that there are six peaks in $\sigma_1(\omega)$ at $\approx$ 149, 166, 325, 456, 566, and 607 cm^{-1}, as well as six peaks in the loss function at $\approx$ 152, 169, 326, 550, 584, and 620 cm^{-1}. As noted previously, these frequencies are not strictly the TO and LO frequencies, due to the mixed nature of the modes.[6] The oscillator strength of the polar mode is usually expressed as[28]

$$\omega_{pi}^2 = \epsilon_\infty(\omega_{\mathrm{LO},i}^2 - \omega_{\mathrm{TO},i}^2) \prod_{i \neq j} \frac{(\omega_{\mathrm{LO},j}^2 - \omega_{\mathrm{TO},i}^2)}{(\omega_{\mathrm{TO},j}^2 - \omega_{\mathrm{TO},i}^2)} \quad (\gamma_{\mathrm{LO},i} = \gamma_{\mathrm{TO},i}). \qquad (13)$$

TABLE I. The values of the mixed LO and TO phonons determined by fitting the factorized form of the dielectric function to the reflectance of sintered CuO (as well as the ^{65}Cu and ^{18}O materials) at 295 K. The measured frequency shifts (%) are determined from the average of the TO and LO shifts. All frequencies are in cm^{-1}.

	$^{63}Cu^{16}O$ mixed LO and TO				$^{65}Cu^{16}O$ mixed LO and TO					$^{63}Cu^{18}O$ mixed LO and TO				
Symmetry	$\omega_{\mathrm{TO},i}$	$\omega_{\mathrm{LO},i}$	$\gamma_{\mathrm{TO},i}$	$\gamma_{\mathrm{LO},i}$	$\omega_{\mathrm{TO},i}$	$\omega_{\mathrm{LO},i}$	$\gamma_{\mathrm{TO},i}$	$\gamma_{\mathrm{LO},i}$	Shift	$\omega_{\mathrm{TO},i}$	$\omega_{\mathrm{LO},i}$	$\gamma_{\mathrm{TO},i}$	$\gamma_{\mathrm{LO},i}$	Shift
A_u^1	166.2	168.5	4.0	4.1	163.4	165.3	5.4	4.7	−1.8	164.3	166.7	6.8	5.6	−1.1
A_u^2	325.3	326.0	4.5	4.3	322.5	323.1	4.0	3.8	−0.9	324.3	324.8	3.9	3.5	−0.3
A_u^3	456	550	67	74	455	534	70	65	−1.7	455	539	82	75	−1.7
B_u^1	149.3	151.6	3.0	3.1	146.7	148.2	2.8	3.4	−2.0	148.2	149.9	3.4	3.4	−0.9
B_u^2	566	584	38	32	561	579	73	55	−0.9	540	556	41	49	−4.7
B_u^3	607	620	31	25	601	611	26	26	−1.2	581	593	46	26	−4.3
	$\epsilon_\infty = 6.3$				$\epsilon_\infty = 6.2$					$\epsilon_\infty = 6.2$				

While the mixed TO-LO nature of the vibrations reduces the applicability of this approach, it is still true that the splitting of the features seen in σ_1 and the loss function is a general indication of the strength of the vibration. The large splitting between the 456 cm^{-1} TO mode and the 550 cm^{-1} LO mode gives rise to the strong reststrahlen band seen in the reflectance.

A detailed lattice-dynamical calculation of the eigenvalues and eigenvectors of the ($\mathbf{q} = 0$) normal modes of CuO has been previously performed.[29] The calculated eigenvectors indicate that the A_u^1, A_u^2, and B_u^1 modes are all mainly Cu vibrations corresponding to "bond-bending" modes. The A_u^3, B_u^2, and B_u^3 modes are predominantly Cu-O vibrations; in particular the B_u^2 and B_u^3 modes are strongly coupled Cu-O stretches along the [101] and [10$\bar{1}$] directions, respectively.

Information about the nature of the phonons may also be obtained from the isotopic shifts caused by ^{65}Cu and ^{18}O substitution. The predicted isotope shifts have been calculated using a simple harmonic model, and are listed in Table II. The experimental shifts for the A_u^1, A_u^2, and B_u^1 modes indicate they are mainly Cu vibrations, in agreement with the first-principles calculation,[29] while shifts for the B_u^2 and B_u^3 modes indicate they are Cu-O stretches. The behavior of the A_u^3 mode is more difficult to characterize, due to the large linewidths (> 60 cm^{-1}) associated with this feature. However, even taking this into account, the observed shift is very small, and in the case of the ^{18}O substitution, well below the calculated shift.

The present work on sintered samples departs from the work of Kliche and Popovic[13] in two significant respects: (i) A strong reststrahlen band is clearly visible and shows a significant softening at T_{N1}, and (ii) no new structure is observed below T_{N1} or T_{N2}. The absence of additional structure in the AF-ordered ground state indicates that despite the doubling of the magnetic unit cell in the a and c directions below T_{N2}, we have not observed any zone-boundary phonons activated by zone folding due to the formation of a superlattice, as was previously proposed.[13] Interestingly, a new feature is observed below T_{N2} in the Raman spectrum at ≈ 240 cm^{-1}. However, it is unclear if this feature is due to zone folding or is magnetic in origin.

A more detailed understanding of the behavior of the phonons in CuO may be gained from the polarized reflectance of single crystals. The dispersion-analysis model (Sec. III) was developed specifically for monoclinic crystals,[22–24] and has been extended to describe the reflectance from the [1$\bar{1}$0] growth plane.[15] The reflectance for $E \parallel c$ and $E \perp c$ on the [1$\bar{1}$0] growth face has been fitted with the modified dispersion-analysis model using a least-squares technique; the two polarizations are fit simultaneously, allowing the A_u and B_u phonons to be refined at the same time. The results of the fit to the reflectance are shown in Fig. 10 at room temperature and 80 K, and show an excellent agreement with the data (the parameters returned by these fits are listed in Table III). In general, the TO frequencies determined in the crystal are no different than those in the sintered powders, with the exception of the B_u^2 and B_u^3 modes, which are both significantly lower in the single crystal. This result suggests that in the sintered powders, the B_u^2 and B_u^3 modes show a more pronounced LO character.

The temperature dependence of $\omega_{TO,i}$, γ_i, and ω_{pi} are shown in Fig. 11 for the three high-frequency TO modes; the three low-frequency phonons display little or no temperature dependence. The softening of the TO mode identified in the sintered samples may now be examined more quantitatively — the softening below T_{N1} is accompanied by an anomalous broadening and increase in the oscillator strength; below T_{N2}, the mode band hardens slightly while narrowing and decreasing in strength.

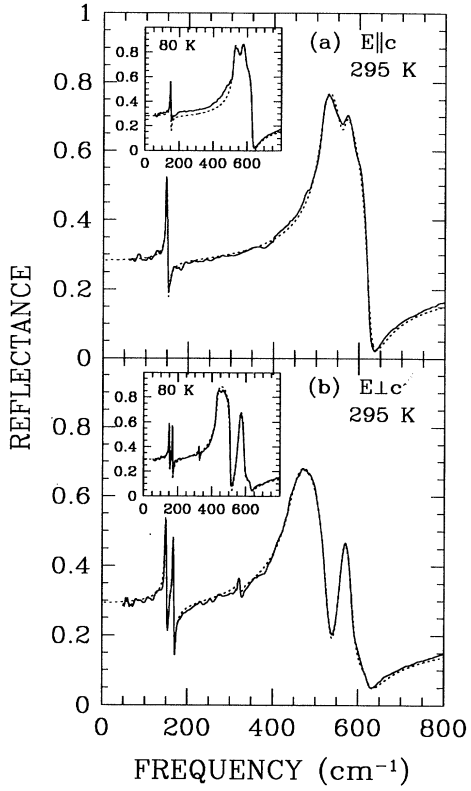

FIG. 10. The fit using the modified dispersion-analysis model (dotted line) to the reflectance from the [1$\bar{1}$0] growth face (solid line). (a) $E \parallel c$ at 295 K. Inset: fit to the data at 80 K. (b) $E \perp c$ at 295 K. Inset: fit to the data at 80 K. The parameters returned by the fits for the two temperatures are listed in Table III.

TABLE II. The calculated isotope shifts (%) for sintered cupric oxide for ^{65}Cu and ^{18}O substitutions. A simple harmonic model is used, $\omega/\omega_0 = (m_0^*/m^*)^{1/2}$, where $m^* = m_a m_b/(m_a + m_b)$ is the reduced mass. The calculation for the mixed Cu-O vibrations assumes equal weights.

	ω/ω_0 (%)	
Vibration	^{65}Cu	^{18}O
Cu-Cu	−1.55	–
Cu-O	−0.31	−4.5
O-O	–	−5.7

TABLE III. The parameters used to fit the dispersion analysis model to the reflectance data for $E \parallel c$ and $E \perp c$ in the $(1\bar{1}0)$ plane. In the model fits, $\epsilon_{xx,\infty} = \epsilon_{yy,\infty} = 6.7$, and $\epsilon_{zz,\infty} = 7.4$. The oscillator angles (ϕ_i) are measured normal to the c axis in the ac plane. The oscillators of the A_u modes are oriented along the b axis. All units are in cm^{-1}, except for the oscillator angles, which are expressed in degrees.

	295 K					80 K				
Symmetry	$\omega_{TO,i}$	$(\omega_{LO,i})^a$	γ_i	ω_{pi}	ϕ_i	$\omega_{TO,i}$	$(\omega_{LO,i})^a$	γ_i	ω_{pi}	ϕ_i
A_u^1	166.5	(169)	2.6	151	—	168.9	(171)	1.9	157	—
A_u^2	323.7	(325)	3.3	107	—	326.1	(327)	2.0	122	—
A_u^3	450	(528)	40	1442	—	433	(505)	11	1390	—
B_u^1	147.6	(151)	1.8	141	37	148.8	(152)	1.5	151	37
B_u^2	516	(620)	19	857	266	522	(625)	8.1	831	261
B_u^3	566	(585)	16	443	139	565	(595)	11	554	140

[a]The values for $\omega_{LO,i}$ have been estimated (to the nearest wave number) from the peaks in the loss function as determined by a Kramers-Kronig analysis, and as such may not be the true LO frequencies.

In contrast, the other two high-frequency phonons show only small frequency anomalies near T_{N2}. There is some broadening of the 566 cm^{-1} B_u^3 mode near T_{N2}, but the 516 cm^{-1} B_u^2 mode narrows with decreasing temperature, showing no broadening near T_{N2}. However, there are large changes in the oscillator strengths; particularly of the 566 cm^{-1} mode, which increases dramatically at T_{N2}. The fitted values for the TO frequencies are in good agreement with the frequencies obtained from fits to the neutron data.[6] Along with the vibrational parameters of the B_u modes, the direction angles ϕ_i were also fit at the same time; for the B_u^1 and B_u^3 modes, the angles

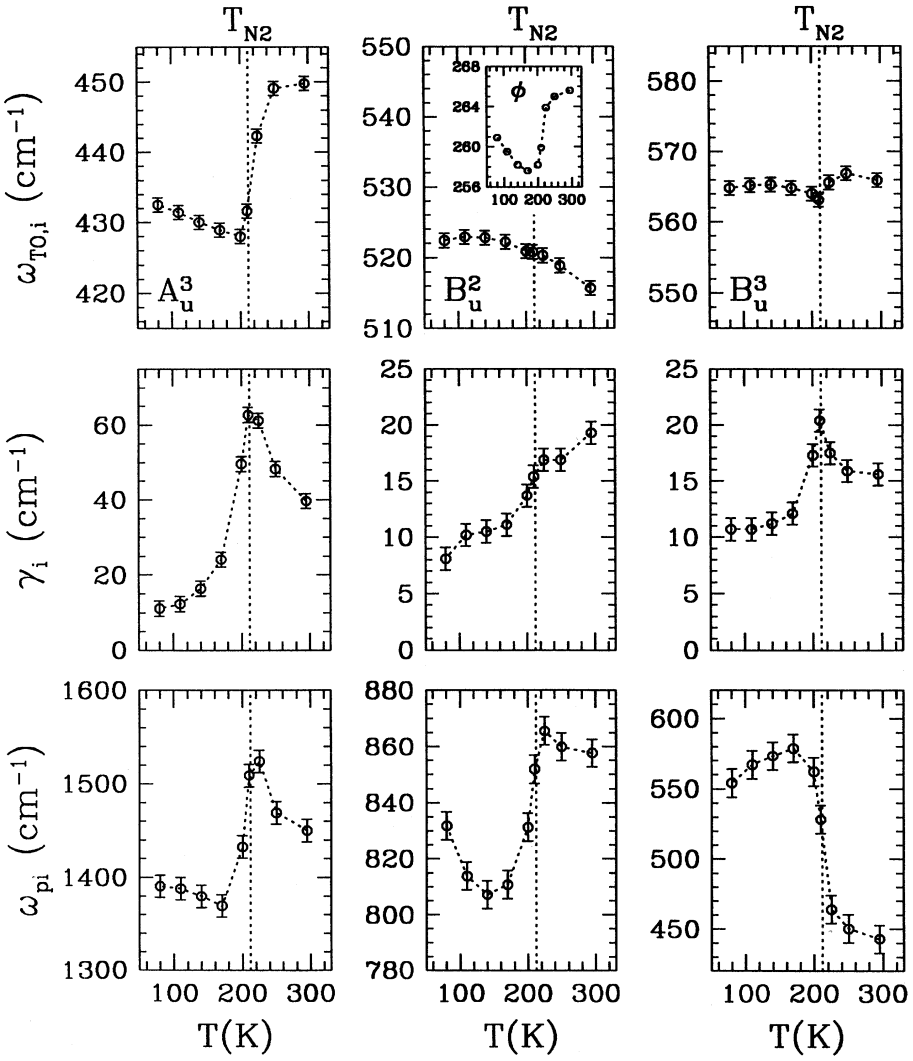

FIG. 11. The temperature dependence of the dispersion-analysis model parameters for the three high-frequency modes, fit simultaneously to the $E \parallel c$ and $E \perp c$ ([$1\bar{1}0$] growth face) reflectance, where $\omega_{TO,i}$, γ_i, and ω_{pi} are the frequency, width, and oscillator strength of the mode. Note the anomalous behavior of many of the parameters near T_{N2}. The inset for the B_u^2 mode shows the temperature dependence of the direction angle ϕ_i.

remained constant. However, the angle for the B_u^2 undergoes a significant change below T_{N1} (shown in the inset for $\omega_{\mathrm{TO},i}$ for B_u^2 in Fig. 11). The change in ϕ_i implies that the atomic displacement vectors of the B_u^2 mode are changing through the Néel transitions; other than a small change in the oscillator strength, the B_u^2 mode displays little else in the way of anomalous behavior. It is also interesting to note that while the oscillator strengths of the three high-frequency phonons are all changing, the combined oscillator strength ($\sum \omega_{pi}^2$) remains approximately constant, indicating a transfer of oscillator strength in the AF-ordered ground state.

The softening of the reststrahlen band near T_{N1}, as well as other phonon anomalies that are observed upon entering the AF-ordered ground state, suggests that the magnetic phase transition is probably accompanied by a weak structural distortion of the Cu-O chains. This would not be an unusual condition, since the superexchange between the Cu ions along the chain is quite large,[6] with an effective exchange constant of $J \simeq 80$ meV (comparable to the interaction energies found in the high-T_c cuprates[30]). The recent structural determination of the low-temperature phase[31] at 195 K, where the Cu-O bonds in the fourfold-coordinated copper atom are observed to change slightly below the Néel transitions, tends to support this point of view. At room temperature, the Cu-O bonds along the [101] direction are of unequal length, differing by ≈ 0.16 Å, while in the low-temperature phase (195 K) the bond lengths along the [101] chains become more equal, with the difference decreasing to ≈ 0.11 Å. This weak distortion appears to be related to the phonon anomalies observed in this material. It has also been suggested that because of the superexchange between the Cu ions, the decrease in the asymmetry of the bond lengths along the [101] direction may lead to increased antiferromagnetic coupling.[31] It would be interesting to study the distortion of the Cu-O bonds around the fourfold planar-coordinated copper atom in more detail near the Néel transition, in order to determine if the temperature dependence of the phonon parameters is reflected in the nature of the structural distortion.

An interesting similarity exists between this work and a study of the c-axis phonons in oxygen-reduced $YBa_2Cu_3O_{6+x}$ ($x \approx 0.6$), where a significant transfer of oscillator strength is also observed among the high-frequency Cu-O phonons (at $T \gtrsim T_c$).[32] In the cuprate systems, this behavior is also thought to be due to a weak structural distortion. It is possible that this transition may in part be driven by antiferromagnetic correlations, which are known to play an important role in the normal-state dynamics of these systems.[33,34] However, it is not clear if these correlations are related to the mechanism for superconductivity in the high-T_c cuprates.

VI. CONCLUSIONS

The reflectance of sintered samples of cupric oxide has been analyzed using the factorized form of the dielectric function. The polarized reflectance ($E \parallel c$, $E \perp c$) measured from the $[1\bar{1}0]$ growth face of a single crystal of CuO has also been analyzed using a modified form of the dispersion-analysis model. In both the sintered powders and the single crystal, the strong reststrahlen band softens below T_{N1}, and is accompanied by a transfer of oscillator strength among the high-frequency Cu-O stretching modes. This behavior is presumably due to a weak structural distortion of the Cu-O chains that accompanies the antiferromagnetically ordered ground state. There are no new vibrational features in the antiferromagnetically ordered ground state, and there is no evidence for the formation of a superlattice in the direct lattice. The similarity between the phonon anomalies in CuO, and the c-axis phonons in oxygen-reduced $YBa_2Cu_3O_{6+x}$, suggests that antiferromagnetic correlations play a role in the weak structural distortion suspected in each of these systems.

ACKNOWLEDGMENTS

We would like to thank P. Joensen for his assistance with the growth of the crystals. We would also like to acknowledge useful discussions with A. McConnell. This work was supported by Simon Fraser University and the Natural Sciences and Engineering Research Council of Canada.

* Present address: Northern Lights College, P.O. Box 1000, Fort St. John, B.C., Canada V1J 6K1.

[1] *Physical Properties of High-Temperature Superconductors*, edited by D. Ginsberg (World-Scientific, Singapore, 1989), and references therein.

[2] J.W. Loram, K.A. Mirza, C.P. Joyce, and A.J. Osborne, Europhys. Lett. **8**, 263 (1989); A. Junod, D. Eckert, G. Triscone, J. Muller, and W. Reichardt, Physica C **162-164**, 478 (1989).

[3] J. Ghijsen, L.H. Teng, J. van Elp, H. Eskes, J. Westerink, G.A. Sawatzky, and M.T. Czyzyk, Phys. Rev. B **38**, 11322 (1989); F. Parmigiani and G. Samoggia, Europhys. Lett. **1**, 543 (1988).

[4] J.B. Forsyth, P.J. Brown, and B.M. Wanklyn, J. Phys. C **21**, 2917 (1988); P.J. Brown, T. Chahopadhyay, J.B. Forsyth, V. Nunez, and F. Tasset, J. Phys. Condens. Matter **3**, 4281 (1991).

[5] B.X. Yang, J.M. Tranquada, and G. Shirane, Phys. Rev. B **38**, 174 (1989); B.X. Yang, T.R. Thurston, J.M. Tranquada, and G. Shirane, *ibid.* **39**, 4343 (1989).

[6] W. Reichardt, F. Gompf, M. Aïn, and B.M. Wanklyn, Z. Phys. B **81**, 19 (1990); M. Aïn, W. Reichardt, B. Hennion, G. Pepy, and B.M. Wanklyn, Physica C **162-164**, 1279 (1989).

[7] W.Y. Ching, Y.N. Xu, and K.W. Wong, Phys. Rev. B **40**, 7684 (1989).
[8] A.A. Samokhvalov, N.N. Loshkareva, Yu. P. Sukhorokov, V.A. Gruverman, B.A. Gizhevskŭ, and N.M. Chebotaev, JETP Lett. **49**, 523 (1989).
[9] J.C. Irwin, J. Chrzanowski, T. Wei, D.J. Lockwood, and A. Wold, Physica C **166**, 456 (1990); J. Chrzanowski and J.C. Irwin, Solid State Commun. **70**, 11 (1989).
[10] H.F. Goldstein, D. Kim, P.Y. Yu, and L.C. Bourne, Phys. Rev. B **41**, 7192 (1990).
[11] H. Hagemann, H. Bill, W. Sadowski, E. Walker, and M. François, Solid State Commun. **73**, 447 (1990).
[12] L. Degiorgi, E. Kaldis, and P. Wachter, Physica C **153-155**, 657 (1988).
[13] G. Kliche and Z.V. Popovic, Phys. Rev. B **42**, 10060 (1990).
[14] S.N. Narang, V.B. Kartha, and N.D. Patel, Physica C **204**, 8 (1992).
[15] S. Guha, D. Peebles, and T.J. Wieting, Phys. Rev. B **43**, 13092 (1991).
[16] M. Born and K. Huang, *Dynamical Theory of Crystal Lattices* (Oxford, London, 1954), p. 117.
[17] B.M Wanklyn and B.J. Garrard, J. Mater. Sci. Lett. **2**, 285 (1983).
[18] S. Åsbrink and L.-J. Norrby, Acta. Crystallogr. B **26**, 8 (1970).
[19] C.C. Homes, M. Reedyk, D.A. Crandles, and T. Timusk, Appl. Opt. **32**, 2976 (1993).
[20] D.W. Lynch and W.R. Hunter, in *Handbook of Optical Constants of Solids*, edited by E.D. Palik (Academic, New York, 1991), p. 286.
[21] L.D. Landau and E.M. Lifshitz, *Electrodynamics of Continuous Media* (Pergamon, Oxford, 1960), p. 324.
[22] M.V. Belousov and V.F. Pavinich, Opt. Spectrosc. **45**, 771 (1978).
[23] V.F. Pavinich and M.V. Belousov, Opt. Spectrosc. **45**, 881 (1978).
[24] V.F. Pavinich and V.A. Bochtarev, Opt. Spectrosc. **65**, 640 (1988).
[25] B. Karlsson, C.G. Ribbing, A. Roos, E. Valkonen, and T. Karlsson, Phys. Scr. **25**, 826 (1982).
[26] F. Gervais and B. Piriou, J. Phys. C **7**, 2374 (1974); Phys. Rev. B **10**, 1642 (1974); J.L. Servoin, F. Gervais, A.M. Quittet, and Y. Luspin, *ibid.* **21**, 2038 (1980).
[27] A.S. Barker, Jr., in *Far-Infrared Properties of Solids*, edited by S.S. Mitra and S. Nudelman (Plenum, New York, 1970), p. 247.
[28] L. Genzel, T.P. Martin, and C.H. Perry, Phys. Status Solidi B **62**, 83 (1974).
[29] J.C. Irwin, T. Wei, and J.P. Franck, J. Phys. Condens. Matter **3**, 299 (1991).
[30] K.B. Lyons, P.A. Fleury, L.F. Schneemeyer, and J.V. Waszczak, Phys. Rev. Lett. **60**, 732 (1988); K.B. Lyons, P.A. Fleury, J.P. Remeika, and T.J. Negran, Phys. Rev. B **37**, 2353 (1988).
[31] S. Åsbrink and A. Waśkowska, J. Phys. Condens. Matter **3**, 8173 (1991).
[32] C.C. Homes, T. Timusk, R. Liang, D.A. Bonn, and W.N. Hardy, Phys. Rev. Lett. **71**, 1645 (1993).
[33] A.J. Millis and H. Monien, Phys. Rev. Lett. **70**, 2810 (1993).
[34] P. Aebi, J. Osterwalder, P. Schwaller, and L. Schlapbach, M. Shimoda, T. Mochiku, and K. Kadowaki, Phys. Rev. Lett. **72**, 2757 (1994).